Temperature Dependence of the Thermo-Optic Coefficient of GeO2-doped Silica Glass Fiber

Gaspar Mendes Rego *

Posted Date: 3 July 2024

doi: 10.20944/preprints202407.0272.v1

Keywords: silica glass; refractive index; material dispersion; thermo-optic coefficient; cryogenic temperatures

Article

Temperature Dependence of the Thermo-Optic Coefficient of GeO_2-Doped Silica Glass Fiber

Gaspar Rego [1,2]

[1] ADiT-LAB, Instituto Politécnico de Viana do Castelo, *Rua Escola Industrial e Comercial Nun'Álvares*, 4900-347 Viana do Castelo, Portugal; gaspar@estg.ipvc.pt

[2] Center for Applied Photonics, INESC TEC, Rua Dr. Roberto Frias, 4200-465 Porto, Portugal

Abstract: In this paper we derived an expression that allows the determination of the thermo-optic coefficient of weakly-guiding germanium-doped silica fibers, based on the thermal behavior of optical fiber devices, such as, fiber Bragg gratings (FBGs). The calculations rely on the full knowledge of the fiber parameters and on the temperature sensitivity of FBGs. In order to validate the results, we estimated the thermo-optic coefficient of bulk GeO_2 glass at 293 K and 1.55 μm to be 18.3×10^{-6} K^{-1}. The determination of this value required to calculate a correction factor which is based on the knowledge of the thermal expansion coefficient of the fiber core, the Pockels' coefficients (p_{11}=0.125, p_{12}=0.258 and p_{44}=-0.0662) and the Poisson ratio (ν=0.161) of the SMF-28 fiber. To achieve that goal, we estimated the temperature dependence of the thermal expansion coefficient of GeO_2 and we discussed the dispersion and temperature dependence of Pockels' coefficients. We have presented expressions for the dependence of the longitudinal and transverse acoustic velocities on the GeO_2 concentration used to calculate the Poisson ratio. We have also discussed the dispersion of the photoelastic constant. An estimate for the temperature dependence of the thermo-optic coefficient of bulk GeO_2 glass is presented for the 200-300 K temperature range.

Keywords: silica glass; refractive index; material dispersion; thermo-optic coefficient; cryogenic temperatures

1. Introduction

Modeling the thermal behavior of fiber gratings in extreme conditions such as at cryogenic temperatures is very important in order to assess the performance of sensor devices. Recently [1], we have discussed the expected values for the thermo-optic coefficient, dn/dT, of silica glass, the main constituent of an optical fiber. In order to obtain dn/dT for the fiber core, we need to know its composition and bear in mind that during fiber drawing, due to the different viscosities of core and cladding materials, stresses will be induced and, therefore, the final refractive index will also be affected. For the sake of simplicity and to control the dopants impact we shall focus on a well-known weakly-guiding fiber, the SMF-28 from Corning which have a GeO_2 dopant concentration less than 4 mol%. Fiber Bragg gratings (FBGs) imprinted in the SMF-28 fiber will be used to extract the temperature behavior of the effective refractive index that will be afterwards related to dn/dT of the fiber core through a set of equations derived for weakly-guiding fibers. Finally, we will use the additivity model to determine the thermo-optic coefficient of bulk GeO_2 glass. Its temperature dependence will be also discussed through the knowledge of FBGs and the thermal expansion coefficient. To validate the obtained results, we will use data from other optical devices such as interferometers.

The paper is organized in three sections. The first is related to weakly-guiding fibers: its full characterization and the derivation of the equation that enables the determination of the core thermo-optic coefficient through the use of the additivity model. The second to fiber Bragg gratings: its effective refractive index, the temperature sensitivity and the determination of the correction factor. The third section is dedicated to the calculation of the correction factor for the SMF-28 fiber as a function of the Poisson ratio and Pockels´coefficients. The analysis requires the correlation of data obtained by using the stimulated Brillouin gain spectrum, the acoustic velocities, whispering gallery modes, the elastic properties of the fiber, the photoelastic coefficient and the thermal expansion

 doi:10.20944/preprints202407.0272.v1

coefficient of the fiber. Finally, we validate the values obtained for the thermo-optic coefficient by comparing with published results achieved by using Fabry-Perot interferometers.

2. Ge-Doped Silica Glass Fiber

In order to properly model fiber gratings we need to characterize the host fiber, namely to have knowledge of the core diameter and of the refractive index difference between the core and cladding regions. The SMF-28 fiber from Corning is one of the most studied standard fibers and the reasons have been pointed out by researchers as being reliable with well-defined parameters and, therefore, having a wide application in optical communications and sensing [2–4]. However, different values can be found in the literature and even the datasheet should be used only as a reference [5–8]. A long the past 40 years several metrological standards have been used to measure the fiber parameters [9–13]. The best practice may recommend to collect the maximum information possible on the fiber and use waveguide equations to correlate the obtained parameters. For instance, the mode field diameter (*MFD*) at a particular wavelength and the cut-off wavelength (λ_c) can be used to estimate the core radius though the Marcuse´s empirical formula [14–17]:

$$MFD = D_{co}\left[0.65 + 0.434\left(\frac{\lambda}{\lambda_c}\right)^{1.5} + 0.015\left(\frac{\lambda}{\lambda_c}\right)^{6}\right], \quad (1)$$

and afterwards the numerical aperture (*NA*) can be determined by using the normalized frequency *V* expression:

$$V = \frac{\pi D_{co}}{\lambda}\sqrt{n_{co}^2 - n_{cl}^2}, \quad (2)$$

by putting V=2.405 and λ=λ_c to yield:

$$NA = \sqrt{n_{co}^2 - n_{cl}^2} = \frac{2.405*\lambda_c}{\pi D_{co}}. \quad (3)$$

On the other hand, one may think that the refractive index profile (RIP) would clarify any potential ambiguity on the fiber parameters determination, but different techniques such as refracted near field (RNF), transmitted near field, transverse interferometric, quantitative phase imaging, reconstruction through tomographic stress measurement profiles, or using atomic force microscopy results in different values [6,18–22]. In fact, considering the most common technique (RNF), and by sweeping the fiber end-face at 0º and 90º may result in different values for $\circledcirc n$ and D_{co}, being the difference larger for the latter. We should recall that fiber cleaving changes the stress distribution which also affects the refractive index [23] and the determination of its absolute value also requires calibration with a fluid of known refractive index. In general for the SMF-28 fiber, $\circledcirc n$ ranges from 4.4-5.4x10^{-3} and D_{co} from 8.0-8.8 μm and the most common values are: $\circledcirc n$=5.2-5.4x10^{-3} and D_{co}=8.2-8.6 μm. Based on our measurements [24], we will consider$\circledcirc\circledcirc n$ ~5.4x10^{-3} and D_{co}~8.6 μm which matches the values presented in [4]. Furthermore, the writing of weak FBGs in the SMF-28 fiber allows one to determine its effective refractive index (n_{eff}) [25] and the obtained results are also consistent with the assumed fiber parameters. The SMF-28 is a weakly-guiding fiber [26] for which the normalized propagation constant can be written as:

$$b = \frac{n_{eff} - n_{cl}}{n_{co} - n_{cl}}, \quad (4)$$

thus

$$n_{eff} = n_{cl} + b\Delta n, \quad (5)$$

or be expressed as a function of the normalized frequency as [27]:

$$n_{eff} = n_{cl} + \left(1.1428 - \frac{0.996}{V}\right)^2 \Delta n. \quad (6)$$

Through the derivative in order to temperature results:

 doi:10.20944/preprints202407.0272.v1

$$\frac{dn_{co}}{dT}=\frac{\frac{dn_{eff}}{dT}+2\left(1.1428-\frac{0.996}{V}\right)\frac{0.996}{V\lambda}\frac{d\lambda}{dT}\Delta n+\frac{dn_{cl}}{dT}\left[\left(1.1428-\frac{0.996}{V}\right)^2-1+\frac{2*0.996n_{cl}\left(1.1428-\frac{0.996}{V}\right)}{V(n_{co}+n_{cl})}\right]}{\left[\left(1.1428-\frac{0.996}{V}\right)^2+\frac{2*0.996n_{co}\left(1.1428\ \frac{0.996}{V}\right)}{V(n_{co}+n_{cl})}\right]}, \quad (7)$$

From the previous equation it can be concluded that one can determine the thermo-optic coefficient of the fiber core by knowing the fiber parameters, the thermo-optic coefficient of the fiber cladding (typically, pure-silica glass) and the temperature dependence of a fiber device, such as, a FBG. On the other hand, the thermo-optic coefficient of the fiber core is related to the thermo-optic coefficients of SiO_2 and GeO_2 by knowing the fractional volume of glass occupied by GeO_2 (m) and using the additivity model [28]:

$$n_{co}=(1-m)n_{SiO2}+mn_{GeO2}, \quad (8)$$

$$\frac{dn_{co}}{dT}=(1-m)\frac{dn_{SiO2}}{dT}+m\frac{dn_{GeO2}}{dT}, \quad (9)$$

being m defined as:

$$m=\frac{\frac{M_{GeO2}}{M_{SiO2}}\frac{\rho_{SiO2}}{\rho_{GeO2}}x}{1+x\left[\frac{M_{GeO2}}{M_{SiO2}}\frac{\rho_{SiO2}}{\rho_{GeO2}}-1\right]}, \quad (10)$$

and x is the molar fraction of GeO_2 dopant concentration.

On contrary to pure silica, published values in the literature for the thermo-optic coefficient of pure GeO_2 [29,30] is scarce and, therefore, this set of equations enables to determine its value, say at room temperature and for a particular wavelength (for instance, 293 K and 1.55 μm). At this point, we shall recall that the refractive index of the core and cladding materials may differ for the preform and for the optical fiber. The differences arise from mechanical and thermal stresses due to the different viscosity and thermal expansion coefficients of core and cladding materials and also from viscoelasticity, due to its time dependence induced during fiber drawing. Typically, the pure silica cladding bears the applied force and it has not enough time to reach thermodynamic equilibrium. The elastic stresses affect mainly the core, that is compressed by the cladding, while viscoelasticity affects mainly the pure silica cladding. Both contributes to a decrease of the refractive index of core and cladding materials in the fiber in comparison to the preform. Taking into account the value of 4.7 MPa [20], for the mean axial stress measured in the SMF-28, the cladding refractive index decrease due to frozen-in viscoelastic stress is calculated to be -3×10^{-5} [31] and can be, therefore, neglected. Furthermore, the residual elastic stresses contribute to a decrease in the cladding refractive index of about -2×10^{-5} and to an increase in the core of about 4×10^{-5} [32,33]. The overall contribution to $\circledcirc n$ is of the order of 1×10^{-4}. On the other hand, it has been claimed that the refractive index of the cladding can be several parts in the 4th decimal place higher than that of annealed silica and that is attributed to quenching of the fiber during its production [9,13]. The reference value for annealed silica is the one obtained by Malitson [34] and it is known that the value obtained by Fleming for a quenched glass is about 3×10^{-4} higher [35]. However, as discussed in our previous paper [1], the values obtained by Leviton *et al.* for four samples of annealed silica glass are even higher than for quenched silica (for instance, the values for Corning 7980 silica sample are about 1×10^{-4} above) [36]. Gathering all the information concerning the fiber fabrication and the errors associated to the measurement of the refractive index profile, it is not possible to clearly state that the refractive index of the silica cladding is higher than for annealed bulk samples. Moreover, it is also known that values of the order of 300 g for the drawing tension can reduce the refractive index of the cladding by about 2×10^{-4} [37]. Returning to the SMF-28 fiber, for which only ~12.5 g (peak stress 10 MPa) are used for the drawing tension, we do not expect considerable changes in the cladding refractive index [23,38,39]. Furthermore, those changes are within the uncertainty of the measurements and in fact, more important than knowing the absolute value of the cladding refractive index is to know the index difference, $\circledcirc n$.

As far as the core is concerned, each 1 mol% GeO_2 accounts for 0.1% in $\circledcirc$ [40] and therefore for $\circledcirc n=5.4\times10^{-3}$ we expect ~3.7 mol% GeO_2. Also, for the core we can question if we should use annealed or quenched GeO_2. Calculations using the Sellmeier´s coefficients for pure GeO_2 (quenched and annealed samples) presented in [41] and for silica, the ones obtained by Leviton and Frey for Corning

 doi:10.20944/preprints202407.0272.v1

7980 [36], show that the difference in values for $\circledcirc n$ is of about 1x10^{-4} being the mol% of GeO_2 3.70±0.04. Therefore, we will also use the GeO_2 annealed sample, resulting in $\circledcirc n$ = 1.464x10^{-3} x [GeO_2(mol%)] at 1.55 μm (valid for small concentrations since the dependence is in fact quadratic, Figure 1).

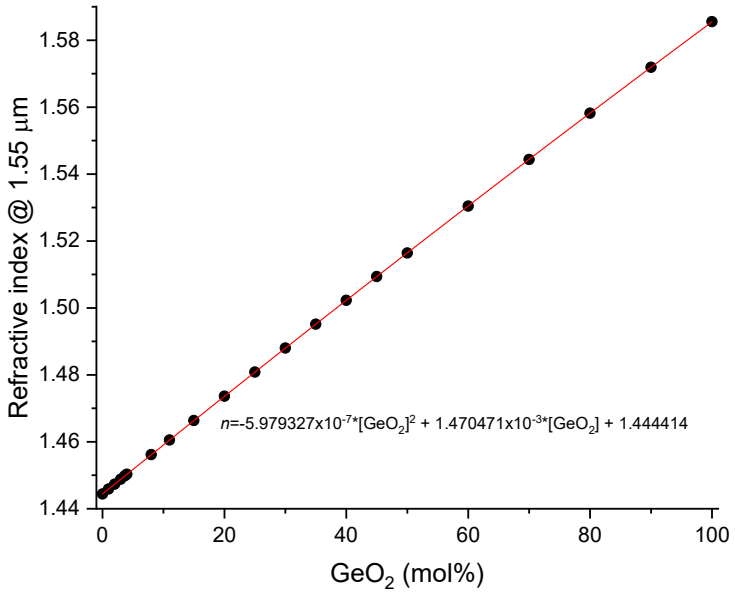

Figure 1. Refractive index of binary SiO_2-GeO_2 glasses at room temperature and 1.55 μm.

3. Fiber Bragg Gratings

The determination of the core thermo-optic coefficient requires the knowledge of the value of the effective thermo-optic coefficient. That, can be accomplished by following the thermal behavior of fiber Bragg gratings by using the temperature dependence of the Bragg wavelength, λ_B:

$$\lambda_B = n_{eff}\Lambda, \tag{11}$$

where n_{eff} is the effective refractive index and Λ the pitch of the phase-mask (which is twice that of the grating period).

The derivative of the grating resonance condition yields:

$$\frac{dn_{eff}}{dT} = n_{eff}\left(\frac{1}{\lambda_B}\frac{d\lambda_B}{dT} - \alpha_{cl}\right), \tag{12}$$

where α_{cl} represents the thermal expansion coefficient of the cladding material. It should be noted that being the cladding much larger than the core and since the thermal expansion coefficient of the core is larger than that of the cladding, it is the latter that defines the expansion of the grating period. On the other hand, the core is not free to expand and thus a compressive stress is induced in the core region during fiber heating leading to an increase of the refractive index. Therefore, the effective refractive index should be corrected by using the following expressions [42–44]:

$$\left(\frac{dn_{eff}}{dT}\right)_{corr} = \frac{n_{eff}^3}{2}\left(2\varepsilon oc_{eff} + \sigma oc_{eff}\right)(\alpha_{co} - \alpha_{cl}), \tag{13}$$

where α_{co} represents the thermal expansion coefficient of the core material, that for the SMF-28 fiber can be calculated using the additivity model resulting in the following expression:

$$\alpha_{SMF28} = \frac{(1-m)\,\rho_{SiO2}\,\alpha_{SiO2} + m\,\rho_{GeO2}\,\alpha_{GeO2}}{\rho_{SMF28}}, \tag{14}$$

and ρ_{SMF28} is the density of the fiber core determined as:

$$\rho_{SMF28} = \rho_{SiO2}(1-m) + \rho_{GeO2}m. \tag{15}$$

The εoc_{eff} *and* σoc_{eff} represent the strain and stress-optic effective coefficients and are expressed as:

 doi:10.20944/preprints202407.0272.v1

$$\varepsilon oc_{eff} = (xn_{GeO2}^3 \varepsilon oc_{GeO2} + (1-x)n_{SiO2}^3 \varepsilon oc_{SiO2}) \frac{1}{n_{eff}^3}, \quad (16)$$

$$\sigma oc_{eff} = (xn_{GeO2}^3 \sigma oc_{GeO2} + (1-x)n_{SiO2}^3 \sigma oc_{SiO2}) \frac{1}{n_{eff}^3}, \quad (17)$$

where n, εoc and σoc represent the values of refractive index, strain and stress-optic coefficients of the bulk materials:

$$\varepsilon oc = p_{12} - \nu(p_{11} + p_{12}), \quad (18)$$

$$\sigma oc = p_{11} - 2\nu p_{12}. \quad (19)$$

The values of molar mass (M), density, thermal expansion coefficient [1], Pockels' photoelastic coefficients (p_{11}, p_{12}) and Poisson ratio (ν) of germanium-doped silica glass are, respectively, presented in Table 1 [45].

Table 1. Physical parameters.

Material	M (g/mol)	ρ (kg/m^3)	α (x10^{-6} K^{-1})	P_{11}	P_{12}	ν
SiO_2	60.08	2200	0.45	0.121	0.270	0.170
GeO_2	104.64	3650	7.7	0.130	0.288	0.212

There is a final issue requiring attention as a result of the fact that during the grating inscription a δn_{co} is induced in the fiber core (averaged over the grating length being half of the amplitude modulation for a grating with a duty-cycle of 0.5) which is larger for strong gratings as the reflectivity approaches 1. Consequently, the effective refractive index will also change. In this context, the induced effective refractive index δn_{eff} can be determined from the grating spectrum by knowing the Bragg wavelength, λ_B the grating length, L and the reflectivity, R and, therefore, δn_{co} can be afterwards obtained by using the confinement factor, η [46,47].

$$\delta n_{eff} = \frac{\lambda_B}{2\pi L} tanh^{-1}\sqrt{R}, \quad (20)$$

$$\delta n_{co} = \frac{\delta n_{eff}}{\eta}, \quad (21)$$

$$\eta = 1 - \frac{1}{V^2}. \quad (22)$$

For the calculations we have assumed the values discussed in the previous section, namely, D_{co}=8.6 μm and Δn=5.4x10^{-3} and for the cladding refractive index at 1.55 μm the value obtained for Corning 7980 (1.4444) [1], by using Eq. (2) and Eq. (6) we determined the effective refractive index for the SMF-28 fiber. Afterwards, by considering a moderate grating (R~24%) [48], and by replacing the values in Eq. (20) – Eq. (22) and Eq. (11), we estimated δn_{eff}, δn_{co} and Λ to be respectively, 4.64x10^{-5}, 5.96x10^{-5} and 1.0729 μm. Then, Eq. (6) – Eq. (19) yields the following values for the thermo-optic coefficients (corrected effective, core and bulk GeO_2): 8.45, 8.55 and 18.3x10^{-6} K^{-1}. In order to validate

 doi:10.20944/preprints202407.0272.v1

our results we have also used a strong grating [49], although in this case we knew the pitch of the phase mask (1.070 μm) but we had to estimate the grating length since it was inscribed on the splice region of two dissimilar fibers being one of them the Corning SMF-28. Based on the knowledge that we had on the impact of the arc discharge on the fiber´s stress annealing (a region of about 1 mm) [50] and also on the separation of the peaks obtained in the Fabry-Perot spectrum ($\circledcirc\lambda=\lambda^2/2n_{co}L$=1 nm) [51] we estimated the grating length to be of ~4.6 mm (the length of the phase mask was 10 mm). Since we had the phase mask pitch we could obtain directly the effective refractive index and apply an iterative method to optimize the value obtained for the induced δn_{co}. In this case the values obtained for the thermo-optic coefficients (corrected effective, core and bulk GeO_2) were 8.48, 8.59 and 19.5x10^{-6} K^{-1}. As can be observed the values are very close to the ones obtained previously for the moderate grating. It should be stressed that the grating temperature sensitivity ($d\lambda/dT$) depends on the fiber (with or without coating and its type), on the wavelength, and on temperature [52]. The values used (9.45 and 9.46 pm/ºC) were obtained for FBGs inscribed in the SMF-28 fiber without coating at ~1.55 μm and at 20 ºC. Care should be taken since the temperature sensitivity depends quadratically on temperature, a fact that sometimes seems to be ignored. We have also tested a strong FBG with a wavelength of 1608.5 nm exhibiting a sensitivity of 9.85 pm/ºC (quadratic fitting between 10 and 50 ºC) [53] and the results obtained were 8.50, 8.62 and 20.1x10^{-6} K^{-1}. The temperature gauge factor $K_T = 1/\lambda_B.d\lambda_B/dT$ of the above gratings increased respectively, from 6.09x10^{-6} K^{-1} to 6.12x10^{-6} K^{-1}, revealing the strong impact of this parameter. Note also that the reference value of 19.4x10^{-6} K^{-1} was obtained at room temperature in the visible region thus, assuming a similar dispersion relation for GeO_2, as for SiO_2, it is expected a value 6% lower at 1.5 μm. Therefore, it is instructive to measure the impact of the different parameters accuracy on the estimation of the bulk GeO_2 thermo-optic coefficient. Starting from typical fiber parameters: D_{co}=5.2-5.4 μm and $\circledcirc n$=5.2-5.4x10^{-3}, differences of the order of ~4% results in relative errors of ~1%. Regarding the thermal expansion coefficient of SiO_2 it is known that it depends on the fictive temperature and on the OH^- content [54,55]. Nevertheless, typical values at room temperature range from 0.40-0.55x10^{-6} K^{-1} [43,56–58]. Common values for type III silica glass at 20ºC can be considered to be (0.47±0.04)x10^{-6} K^{-1} [59–62]. For GeO_2 at room temperature we shall consider 6.9x10^{-6} K^{-1} [63] (typical average value from 25 ºC up to 300 ºC: 7.5x10^{-6} K^{-1} [64–68]). Considering the uncertainty of 8.5% in the thermal expansion coefficient of silica glass, it impacts ~11% the value of the thermo-optic coefficient of GeO_2 glass through Eq. (12)-(13). On the other hand, the difference in determining the grating temperature sensitivity at 20 ºC through a linear or quadratic fitting, results in an uncertainty of 6.3% that leads to a 100% variation in the value of the thermo-optic coefficient of GeO_2 glass. Being aware of that fact, a ~0.45 mm weak-FBG (R<0.1%) was inscribed in the SMF-28 fiber, where a single pulse of 3 mJ at 248 nm was used through a phase mask of 1065.39 nm. The FBG has a resonance wavelength of 1541.58 nm having, therefore, an effective refractive index of 1.446964. The thermal behavior of the FBG was studied from 5 ºC up to 95 ºC and after fitting with a second order polynomial we obtained a value of 9.454 pm/ºC at 20 ºC. Figure 2 shows the temperature dependence of K_T for this grating. For this weak-FBG, the former values of the thermal expansion coefficients would lead to thermo-optic coefficients (corrected effective, core and bulk GeO_2): 8.52, 8.63 and 20.4x10^{-6} K^{-1}, while the new values (0.47x10^{-6} K^{-1} and 6.9x10^{-6} K^{-1}) lead to 8.46, 8.55 and 18.3x10^{-6} K^{-1}. The latter corresponds to a 6% reduction going from visible to the infrared, as observed for bulk SiO_2. The value of the effective dn/dT (without correction) is 8.20x10^{-6} K^{-1}. Applying to the temperature dependence of the Bragg wavelength a similar analysis as the one presented in [69], that is, considering that the period of the phase mask increases linearly with temperature and the refractive index has a quadratic behavior (the reference is 20ºC), yields a value of 8.25x10^{-6} K^{-1} (0.6% higher). The core's thermo-optic coefficient increases linearly with GeO_2 concentration (mol%) at a ratio of ~0.106. Recently [53], it was suggested that the cladding of the SMF-28 fiber would have similar thermo-optic coefficients as the Suprasil glass. However, based on our results for Suprasil 3001 [1], this would lead to a thermo-optic coefficient of bulk GeO_2 of 11.56x10^{-6} K^{-1}, which is not correct. Therefore, the reason for the discrepancy lays in the higher values obtained for K_T as a consequence of the linear fitting applied to the Bragg wavelength.

 doi:10.20944/preprints202407.0272.v1

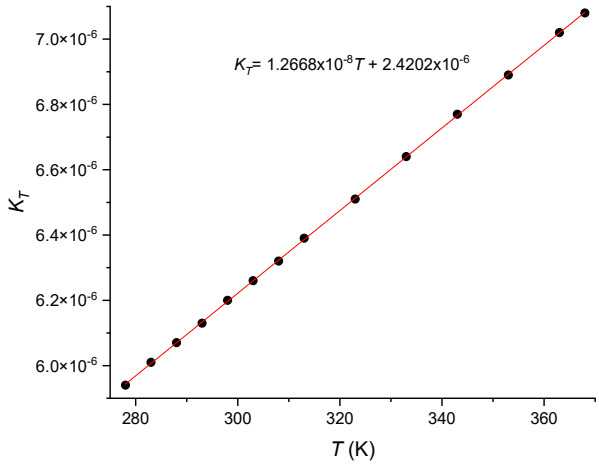

Figure 2. Temperature gauge factor of a weak-FBG.

As a final remark, note that different values can be found in the literature for the parameters ν, p_{11} and p_{12} since they may depend on temperature, wavelength and if it is a bulk or fiber glass. Therefore, in the next section we will present another approach to obtain the correction factor, $\frac{dn_{eff}}{dT}_{corr}$.

4. Effective Parameters ν, p_{11} and p_{12} for the SMF-28 Fiber

The correction factor will be determined by using Eq. (13) through the parameters for the SMF-28 fiber. The Poisson ratio, for the fiber cladding is obtained by applying the following expression:

$$\nu = \frac{1-2\left(\frac{v_S}{v_L}\right)^2}{2\left(1-\left(\frac{v_S}{v_L}\right)^2\right)}, \tag{23}$$

where v_S e v_L are the transverse and longitudinal acoustic velocities and can be determined by knowing the cladding radius [70]:

$$\frac{v_S}{R_{cl}} = 59.345 \pm 0.009\ m/(s.\mu m), \tag{24}$$

$$\frac{v_L}{R_{cl}} = 94.463 \pm 0.006\ m/(s.\mu m). \tag{25}$$

Thus, ν for SiO_2 cladding is obtained by the ratio of the acoustic velocities yielding 0.1740±0.0002 at 20 ºC. To determine Pockels' coefficients for silica cladding we followed the procedure presented in [32], that relies on the strain dependence of TE and TM polarized whispering gallery modes (WGM) resonances. The Pockels' coefficients were determined for two wavelengths, 1.064 μm and 1.55 μm. When using the obtained values for the calculation of the photoelastic constant, C, we found that it would be larger at the longer wavelength, what is not correct (to be discussed below) [71–73]. Thus, by careful analysis of the figures in [32] and [74], we realized that the slopes in those figures were incidentally interchanged. Therefore, the correct values at 1.064 μm and 1.531 μm are: p_{11}=0.113, p_{12}= 0.250 and p_{44}=-0.0685 and p_{11}=0.130, p_{12}= 0.265 and p_{44}=-0.0676, respectively. It is interesting to note that the coefficients are essentially wavelength independent in the 3rd telecommunication window: $dp_{11}/d\lambda$=3.66x10^{-5} nm^{-1}, $dp_{12}/d\lambda$=3.28x10^{-5} nm^{-1} and $dp_{44}/d\lambda$=1.93x10^{-6} nm^{-1}. The signs of the wavelength dependence of Pockels' coefficients compare fairly well in the visible and near infrared range [72,73]. For the sake of further comparison (we will use instead the stress-optic rotation coefficient, g defined below by Eq. 32), the latter value corresponds to $dg/d\lambda$=-0.069g/λ nm^{-1}, which is in excellent agreement with the value of -0.069g/λ obtained for a silica fiber core-doped with 3.4 mol% GeO_2 and B_2O_3 co-doped cladding, in the 1.064-1.3 μm wavelength range [75]. On the other hand, for a pure

 doi:10.20944/preprints202407.0272.v1

silica-core fibers and B_2O_3 co-doped cladding a value of -0.056g/λ nm^{-1} was obtained in the 630-880 nm [76] and for dispersion-shifted fibers (DSF) dg/dλ=-0.090g/λ nm^{-1} at 1.55 μm [77].

As far as the core is concerned, a more laborious path is required. First, it should be mentioned that the cladding diameter was not measured and the specifications of Fibercore SM1500 4.2/125 states that the cladding as a 2 μm uncertainty. Therefore, using the nominal radius of 62.5 μm and Eq. (24)-(25) yields values of v_L=5940±95 m/s and v_S=3709±60 m/s, respectively. On the other hand, for the same fiber, the echo of the longitudinal and transverse acoustic waves reflecting at the cladding/coating interface repeats at a periodicity of ~21 ns and ~33 ns (with a 0.1 ns resolution) [78], leading to velocity values around 5952 m/s and 3788 m/s. Due to discrepancy, we will proceed through the analysis of the stimulated Brillouin gain spectrum (SBS). The longitudinal acoustic velocity,v_L can be related to the Brillouin frequency shift, f_B through the following equation [79]:

$$f_B = \frac{2n_{eff}v_L}{\lambda_p}, \tag{26}$$

where n_{eff} is the effective refractive index and λ_P the pump wavelength. We have used data corresponding to three germanium-doped silica fibers (3.65 and 8 mol% GeO_2) [79], being one the SMF-28 fiber (3.67 mol% GeO_2) [80–82]. We have also corrected the effect of the drawing tension on the Brillouin frequency shift (-42 MHz/100g) considering a drawing tension similar to the one used in the SMF-28 fiber [83]. Table 2 summarizes the results at 20ºC.

Table 2. SBS and acoustic velocity.

GeO_2 concentration (mol%)	Brillouin frequency, f_B (GHz)	Longitudinal velocity, v_L (m/s)
0	11.143 (extrapolated)	5986.5 (extrapolated)
3.65	10.872	5819.5
3.67	10.863	5818.5
8.0	10.542	5620.3

It should be mentioned, that, we have limited the maximum value of GeO_2 core-dopant concentration in order to calculate the effective indices through the above equations valid for weakly-guiding fibers. Care should also be taken since the Brillouin frequency shift/velocity depends on several fiber properties [84]. The extrapolated value obtained for silica glass is in good agreement with the 5990±10 m/s referenced in [28,85] and it also corresponds to the value obtained for the L_{04} longitudinal acoustic mode at 20ºC (5987 m/s) [86]. The value obtained for the SMF-28 fiber is also a common accepted one (5820 m/s) [87]. Following Koyamada *et al.* [88] relation between longitudinal velocity and GeO_2 concentration ([GeO_2] < 20 mol%) we obtain:

$$v_L = 5987(1 - 7.7x10^{-3} * C_{GeO2}). \tag{27}$$

In which concerns the transverse velocity we determine v_S in silica from Eq. (23) yielding a value of 3761 m/s. Note that a value of 3764 m/s was also obtained through analysis of leaky surface acoustic waves in several Corning silica samples [89]. It is interesting to note that using these values (5987 m/s and 3761 m/s) we find R_{cl}=63.4 μm being within the accuracy stated in the fiber´s specifications. It should be stressed that although in [88] it was considered the concentration in wt%, in fact it should be mol% [90]. Also, the fibers used as one of the references [91] for the Koyamada´s equations contains B_2O_3 in the cladding, with different concentrations, affecting the values obtained for the velocities. As a first guess, we estimated a value of 3673 m/s for v_S in the SMF-28 fiber:

$$v_S = 3761(1 - 6.4x10^{-3} * C_{GeO2}), \tag{28}$$

and, therefore, the Poisson ratio for the SMF-28 fiber would be 0.169.

The elastic properties of materials, longitudinal and shear modulus, M and G, respectively, can be determined directly from the knowledge of the acoustic velocities:

$$M = \rho v_L^2, \tag{29}$$

 doi:10.20944/preprints202407.0272.v1

$$G = \rho v_S^2. \quad (30)$$

On the other hand, the Young´s modulus, E, can be related to M through the Poisson´s ratio ν:

$$\frac{M}{E} = \frac{1-\nu}{(1+\nu)(1-2\nu)}. \quad (31)$$

Therefore, for SiO_2 we get M=78,86 GPa, E=73,08 GPa and G=31,12 GPa. For the SMF-28 fiber M=76,36 GPa and E can be estimated by knowing the effect of GeO_2 concentration on Young´s modulus [64]. A decrease of ~0.35 GPa/mol% was found for GeO_2 concentrations up to 4 mol%, although the temperature and density should be corrected [92]. On the other hand, from results presented in [93] a value of -0.4 GPa/mol% can be determined. Therefore, we estimate E=71.61 GPa for the SMF-28 fiber which is in excellent agreement with the value measured for an SMF without coating, E=71.63±0.43 [94]. A lower value was obtained for the SMF-28e (70.05±0.34) [95], however it requires a precise measurement of the fiber cladding diameter which was not performed. Moreover, by applying the additivity model and by using data related to pure bulk SiO_2 and GeO_2 from [96] results a value E=71.65 GPa which, once again, validates our result. For the sake of completion, the model can be improved by considering other factors such as the dissociation energy and ionic radius [97–99]. From the values of E and M for the SMF-28 fiber results ν=0.1612, also in accordance to [93] and thus v_S =3698 m/s. Therefore, Eq. (28) should be corrected to be

$$v_S = 3761(1 - 4.6x10^{-3} * C_{GeO2}). \quad (28^*)$$

It should be highlighted that the obtained Poisson´s ratio is lower for GeO_2 doped silica glass fibers which also agrees with [91], but it is in contradiction to what is expected by applying the additivity model to bulk glasses [100]. We are aware that the results obtained depend on the initial values, but by following the existing interconnection between several parameters allows us to validate the results. We shall now work, with Pockels' coefficients (p_{11}, p_{12} and p_{44}), stress-optic rotation coefficient (g) and photoelastic constants (C=C_1-C_2). The coefficient g can be determined through twist/rotation measurements and is related to p_{44} through the equation:

$$g = -n^2 p_{44}, \quad (32)$$

and

$$C = C_1 - C_2 = \frac{n^3 p_{44}}{2G}, \quad (33)$$

where the photoelastic constants, longitudinal C_1 and transverse C_2 are defined as:

$$C_1 = \frac{n^3(p_{11} - 2\nu p_{12})}{2E}, \quad (34)$$

$$C_2 = \frac{n^3(p_{12} - \nu(p_{11} + p_{12}))}{2E}. \quad (35)$$

Note that g is related to C and p_{44}=(p_{11}- p_{12})/2. Through the use of whispering gallery modes [32] we achieved a value of g=0.141 at 1.55 μm. In general, values for SMF range from 0.140 to 0.144 [101–103]. We also found a value for the SMF-28 fiber [104] that may be 0.139±0.002, since the slope taken from Figure 3 of that paper is at least 69.3x10^{-3} and not 63.9x10^{-3} as stated in the document. Thus, by applying Eq. (32) we obtain p_{44}=-0.0662 and by using the value of 0.205±0.004 for the effective strain-optic coefficient p_{eff} reported in the strain measurements of FBGs [105,106]:

 doi:10.20944/preprints202407.0272.v1

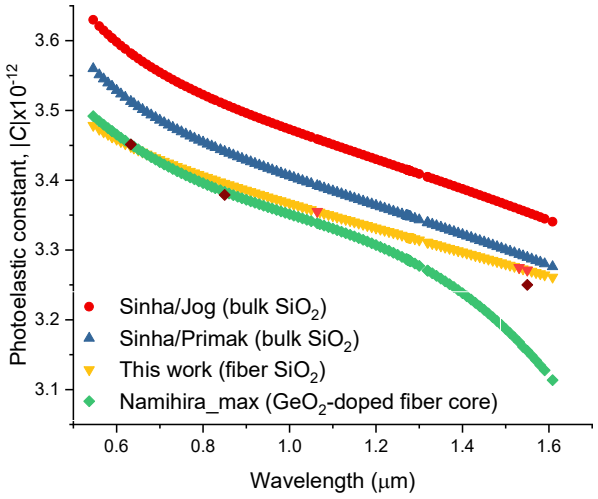

Figure 3. Dispersion of the photoelastic constant for SiO_2 and SiO_2-GeO_2 glasses.

$$p_{eff} = \frac{EC_2}{n} = \frac{n_{eff}^2}{2}\left(p_{12} - \nu(p_{11}+p_{12})\right), \tag{36}$$

we found for the SMF-28 fiber, p_{11}=0.1251, p_{12}= 0.2575. Table 3 summarizes the results for SiO_2 and the SMF-28 fiber. Inserting the values in Eq. (13) results a value for the correction factor that differs only in the fourth decimal place when compared to the initial one. Therefore, we conclude that the major factor that impacts the value of the thermo-optic coefficient is the temperature sensitivity of the FBGs.

Table 3. Physical parameters calculated for SiO_2 and the SMF-28 fiber @1.55 μm.

	SiO_2	SMF-28 (3.67 mol% GeO_2)
n_{cl} or n_{eff}	1.444414	1.446973
p_{11}	0.130	0.125
p_{12}	0.266	0.258
p_{44}	-0.0676	-0.0662
g	0.141	0.139
C_1(Pa^{-1})	7.81×10^{-13}	8.90×10^{-13}
C_2(Pa^{-1})	4.06×10^{-12}	4.14×10^{-12}
C(Pa^{-1})	-3.27×10^{-12}	-3.25×10^{-12}
M(GPa)	78.86	76.36
E(GPa)	73.08	71.63
G(GPa)	31.12	30.83
ν	0.174	0.161

It is instructive to note that if we consider for the SMF-28 fiber a value of g=0.141 [103], it would result in p_{44}=-0.0672 and C=-3.30×10^{-12} Pa^{-1}. Thus, due to the uncertainty in all calculations, the best we can say is that the photoelastic constant for the SMF-28 fiber is very close to the one obtained for pure silica cladding fiber, which is also in excellent agreement with previous results [107,108]. Sinha [109] proposed an expression for the dispersion of the photoelastic constant of fused silica by fitting data from Jog and Krishnan [71] and from Primak and Post [110].

$$C_\lambda = C_{\lambda_0}\frac{n_{\lambda_0}}{n_\lambda}\frac{\lambda^2}{\lambda_0^2}\frac{(\lambda_0^2-\lambda_1^2)}{(\lambda^2-\lambda_1^2)}\frac{(\lambda^2-\lambda_2^2)}{(\lambda_0^2-\lambda_2^2)}, \tag{37}$$

where λ_1=0.1215 μm and λ_2=6.900 μm and the normalization was considered at 0.541 μm to be C=3.63 and 3.56 (absolute value in brewster=10^{-12} Pa^{-1}) for each data set, respectively. Figure 3 shows the dispersion of the photoelastic constants for bulk fused silica (Jog and Primak), for fiber cladding

 doi:10.20944/preprints202407.0272.v1

(calculated in this work) and for low concentration GeO_2-doped silica fiber [108]. For the latter, another expression was fitted to the experimental (maximum) values:

$$C_\lambda = 3.99565 - 1.72552\lambda + 1.5246\lambda^2 - 0.0708\lambda^3. \quad (38)$$

It can be observed that the photoelastic constants are lower for optical fibers when compared to bulk samples and that the values for the core region (doped with low concentrations of GeO_2) are lower than the ones obtained for the cladding. From the experimental values and due to uncertainty [108] it is not possible to clearly state that GeO_2 increases/decreases the value of the photoelastic constant despite it seems that it affects g [103] and, therefore, p_{44} and ultimately C. Since Eq. (38) deviates from the expected values above 1.1 μm, we estimated the dispersion of C by assuming a linear dependence of p_{44} for the whole spectral range. Considering the uncertainty in values of C, at shorter wavelengths, for the Ge-doped fibers [108], they might be slightly lower than for the silica cladding.

The temperature dependence of Pockels' coefficients can be obtained from the temperature derivative of Eq. (33) and from SBS spectrum [90]:

$$g_0 = \frac{2\pi n^7 p_{12}^2}{c\lambda_p^2 \rho v_{L\Delta f}}, \quad (39)$$

where c is the light speed, λ_p is the pump wavelength, Δf is the spectral width and g_0 the intensity. Considering that the product intensity-spectral width is temperature independent [90], results:

$$v_L \alpha n^7 p_{12}^2, \quad (40)$$

and therefore,

$$\frac{1}{v_L}\frac{dv_L}{dT} = 7\frac{1}{n}\frac{dn}{dT} + 2\frac{1}{p_{12}}\frac{dp_{12}}{dT}. \quad (41)$$

Since the temperature derivative of the acoustic velocity is ~0.57 [70] and that the normalized thermo-optic coefficient equals 5.65×10^{-6} K^{-1} [1], yields $dp_{12}/dT=0.74\times10^{-5}$ K^{-1}.

From Eq. (30) and Eq. (33), results:

$$\frac{1}{p_{44}}\frac{dp_{44}}{dT} = 2\frac{1}{v_S}\frac{dv_S}{dT} + \frac{1}{C}\frac{dC}{dT} - 3\frac{1}{n}\frac{dn}{dT}, \quad (42)$$

taking into consideration that $dv_S/dT=0.22$ [70] and that $(1/C)dC/dT = 1.34\times10^{-4}$ K^{-1} [75], yields $dp_{44}/dT=-1.57\times10^{-5}$ K^{-1}. Finally, from the relation between the Pockels' coefficients, $dp_{12}/dT=-2.40\times10^{-5}$ K^{-1}. The temperature dependence of the Poisson ratio is $d\nu/dT=3.76\times10^{-5}$ K^{-1} [70]. Due to the weak dependence on temperature exhibited by the Pockels' coefficients and Poisson ratio, the correction factor is essentially dominated by the difference in the thermal expansion coefficients of the core and cladding. Figure 4 shows the thermal expansion coefficient for pure silica and the SMF-28 fiber. As can be observed the difference between the two curves decreases as the temperature decreases and, consequently, the correction factor also decreases. The thermal expansion coefficient for the SMF-28 fiber was obtained through the use of the additivity model (<4 mol% GeO_2) [43,111,112] where for GeO_2 glass [113,114] we have used data from [115,116] but with fix values at very low temperatures [117], 293 K [63] and 473 K [118]. Following this procedure, data was fitted with an equation similar to the one used by Okaji *et al.* [57] for SiO_2 glass being the coefficients 1.27, 82.42, 1.23, 8.85 and 522.8, respectively. As a final remark, it should be mentioned that without the correction factor, the effective thermo-optic coefficient for the core (SMF-28 fiber) and cladding would be essentially the same. Figure 5 was obtained by using Eq. (6), Eq. (7) and Eq. (12), the values adjusted of K_T from [119] and the temperature dependence of the SiO_2 from [1]. An estimative for the temperature dependence of the thermo-optic coefficient is presented in Figure 6, where we have assumed a linear dependence on temperature for Pockels' coefficients and Poisson ratio [70].

 doi:10.20944/preprints202407.0272.v1

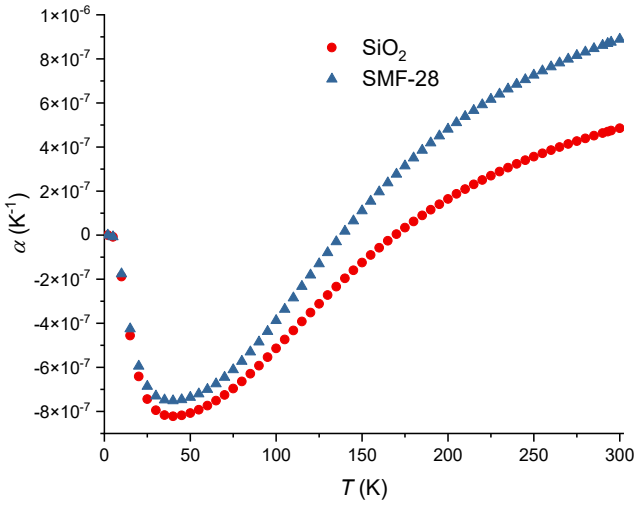

Figure 4. Thermal expansion coefficients for SiO_2 and SMF-28 fiber.

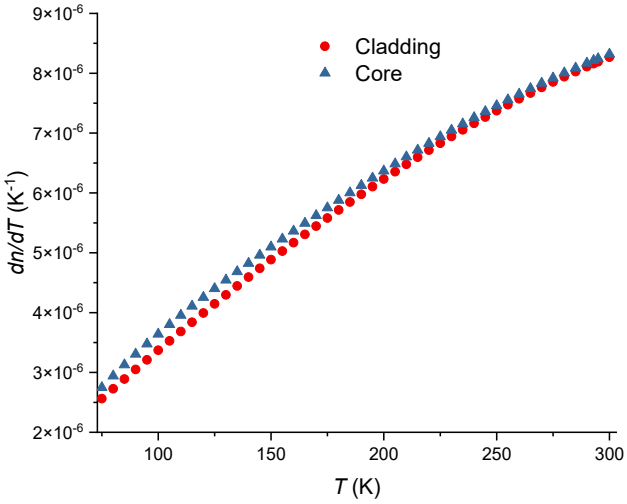

Figure 5. Thermo-optic coefficients for the cladding and core of the SMF-28 fiber.

 doi:10.20944/preprints202407.0272.v1

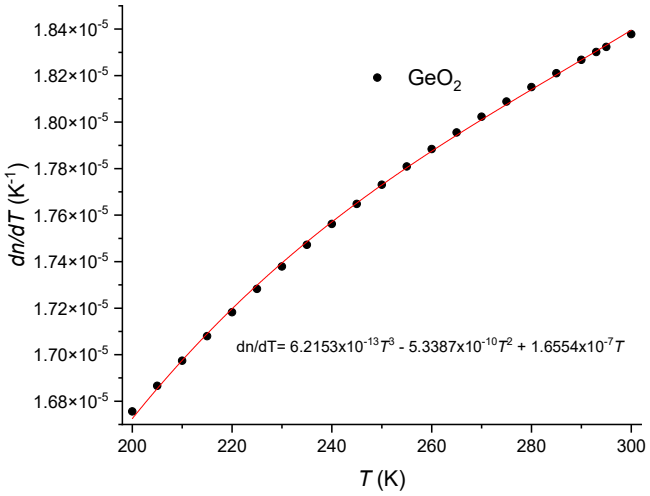

Figure 6. Thermo-optic coefficient for bulk GeO_2 glass.

Other potential techniques to determine the thermo-optic coefficient of an optical fiber are based, for instance, on Fabry-Perot interferometers (FPI) [120–124], Rayleigh backscattering [125–127] and optoelectronic oscillations [128,129]. FPI is the most used approach and thus, for the sake of comparison we estimated from [121] a value of 8.22×10^{-6} K^{-1} for the effective thermo-optic coefficient of a standard fiber, being therefore in excellent agreement (with the value, without correction, obtained in the previous section). On the other hand, following the procedure presented in [120] the values ranged from 8.10×10^{-6} K^{-1} (average heating cycles) up to 8.70×10^{-6} K^{-1} (first heating up). The reasons for the discrepancy are related with two facts: first, the reference temperature, 20ºC, is the lower limit of the temperature interval of the experiment causing uncertainties to the derivative of the fitting equation; second, heating successively above 600 ºC makes irreversible changes to the glass structure which affects the temperature sensitivity and, consequently, the thermo-optic coefficient.

5. Conclusions

We have derived an expression that allows to determine the thermo-optic coefficient of weakly guiding fibers. Our analysis was based on FBG although it can also be used for FPI and Rayleigh scattering. We concluded that the thermo-optic coefficient (effective) of the SMF-28 fiber and of the cladding are essentially the same if one does not consider the correction factor. We estimated the thermo-optic coefficient of the bulk GeO_2 glass from 200 K up to 300 K being 18.3×10^{-6} K^{-1} at 293 K and 1.55 μm We obtained an expression for the temperature dependence of the thermal expansion coefficient of GeO_2-doped silica fibers. Expressions for the transverse and longitudinal acoustic velocities as a function of GeO_2 concentration were also presented. We have determined values for the Poisson ratio, the Pockels' coefficients and photoelastic constant for the SMF-28 fiber. We have also discussed the dispersion and temperature dependence of Pockels' coefficients. We are aware of the uncertainty of some values used, however this paper presents the relations between the different parameters that allow a straightforward correction, if required. Therefore, currently we are investigating the temperature sensitivity of FBGs inscribed, with femtosecond and UV laser radiation, in fibers with different GeO_2 concentration and we are also researching the effect of the Bragg wavelength, hydrogen loading and reflectivity, and the results will be published elsewhere.

Funding: This work was financed by national funds through the Portuguese funding agency, FCT-Fundação para a Ciência e a Tecnologia, within project LA/P/0063/2020.

Institutional Review Board Statement: Not applicable.

Informed Consent Statement: Not applicable.

Data Availability Statement: The data segments can be obtained by contacting the corresponding author.

Acknowledgments: The author would like to express its gratitude to Ignacio Del Villar, J. J. Imas, Rogério Nogueira and Ricardo Oliveira for providing FBGs' data.

Conflicts of Interest: The authors declare no conflicts of interest.

References

1. Rego, G. *Temperature Dependence of the Thermo-Optic Coefficient of SiO2 Glass*. Sensors, 2023. **23**, DOI: 10.3390/s23136023.
2. Kouskousis, B., et al., *Quantitative phase and refractive index analysis of optical fibers using differential interference contrast microscopy.* Applied Optics, 2008. **47**(28): p. 5182-5189.
3. Boilard, T., R. Vallée, and M. Bernier, *Probing the dispersive properties of optical fibers with an array of femtosecond-written fiber Bragg gratings.* Scientific Reports, 2022. **12**(1): p. 4350.
4. Drouin, A., et al., *Spatially resolved cross-sectional refractive index profile of fs laser-written waveguides using a genetic algorithm.* Optics express, 2019. **27**(3): p. 2488-2498.
5. Yablon, A.D., *Multi-Wavelength Optical Fiber Refractive Index Profiling by Spatially Resolved Fourier Transform Spectroscopy.* Journal of Lightwave Technology, 2010. **28**(4): p. 360-364.
6. Bélanger, E., et al., *Comparative study of quantitative phase imaging techniques for refractometry of optical waveguides.* 2018. **26 13**: p. 17498-17510.
7. Mangini, F., et al., *Experimental observation of self-imaging in SMF-28 optical fibers.* Optics Express, 2021. **29**(8): p. 12625-12633.
8. Wang, P., M.H. Jenkins, and T.K. Gaylord, *Arc-discharge effects on residual stress and refractive index in single-mode optical fibers.* Applied Optics, 2016. **55**(9): p. 2451-2456.
9. Raine, K.W., J.G.N. Baines, and D.E. Putland, *Refractive index profiling-state of the art.* Journal of Lightwave Technology, 1989. **7**(8): p. 1162-1169.
10. Gisin, N., R. Passy, and B. Perny, *Optical fiber characterization by simultaneous measurement of the transmitted and refracted near field.* Journal of Lightwave Technology, 1993. **11**(11): p. 1875-1883.
11. Chavez-Gutierrez, F., et al., *Measurement of optical fiber parameters and thermal core diffusion characteristics by digital image processing.* Applied Optics, 2018. **57**(15): p. 4331-4336.
12. Martinez, F. and C. Hussey, *(E)ESI determination from mode-field diameter and refractive index profile measurements on single-mode fibres.* Optoelectronics, IEE Proceedings J, 1988. **135**: p. 202-210.
13. Young, M., *Optical fiber index profiles by the refracted-ray method (refracted near-field scanning).* Applied Optics, 1981. **20**(19): p. 3415-3422.
14. Bayuwati, D., T.B. Waluyo, and I. Mulyanto, *Determination of the effective cut-off wavelength of several single-mode fiber patchcords.* Journal of Physics: Conference Series, 2018. **985**(1): p. 012002.
15. Marcuse, D., *Gaussian approximation of the fundamental modes of graded-index fibers.* Journal of the Optical Society of America, 1978. **68**(1): p. 103-109.
16. Çelikel, O., *Mode field diameter and cut-off wavelength measurements of single mode optical fiber standards used in OTDR calibrations.* Optical and Quantum Electronics, 2005. **37**(6): p. 587-604.
17. Schermer, R.T. and J.H. Cole, *Improved Bend Loss Formula Verified for Optical Fiber by Simulation and Experiment.* IEEE Journal of Quantum Electronics, 2007. **43**(10): p. 899-909.
18. Kokubun, Y. and K. Iga, *Refractive-index profile measurement of preform rods by a transverse differential interferogram.* Applied Optics, 1980. **19**(6): p. 846-851.
19. Raine, K.W., J.G. Baines, and R.J. King *Comparison of refractive index measurements of optical fibres by three methods*. IEE Proceedings J (Optoelectronics), 1988. **135**, 190-195.
20. Hutsel, M.R. and T.K. Gaylord, *Concurrent three-dimensional characterization of the refractive-index and residual-stress distributions in optical fibers.* Applied Optics, 2012. **51**(22): p. 5442-5452.
21. Jenkins, M. and T. Gaylord, *3D Characterization of the Refractive-Index and Residual-Stress Distributions in Optical Fibers*. 2012.
22. Pace, P., et al., *Refractive index profiles of Ge-doped optical fibers with nanometer spatial resolution using atomic force microscopy*. 2004. **12 7**: p. 1452-7.
23. Hutsel, M.R., R. Ingle, and T.K. Gaylord, *Accurate cross-sectional stress profiling of optical fibers.* Applied Optics, 2009. **48**(26): p. 4985-4995.
24. Rego, G.M., J.L. Santos, and H.M. Salgado, *Refractive index measurement with long-period gratings arc-induced in pure-silica-core fibres.* Optics Communications, 2006. **259**(2): p. 598-602.
25. Juelich, F. and J. Roths. *OP2 - Determination of the Effective Refractive Index of Various Single Mode Fibres for Fibre Bragg Grating Sensor Applications*. 2009.
26. Gloge, D., *Weakly Guiding Fibers.* Applied Optics, 1971. **10**(10): p. 2252-2258.
27. Snyder, A.W. and F. Rühl, *Single-mode, single-polarization fibers made of birefringent material.* Journal of the Optical Society of America, 1983. **73**(9): p. 1165-1174.
28. Dragic, P.D. *Simplified model for effect of Ge doping on silica fibre acoustic properties*. Electronics Letters, 2009. **45**, 256-257.

 doi:10.20944/preprints202407.0272.v1

29. Pan, G., et al., *Thermo-optic coefficient of B2O3 and GeO2 co-doped silica fibers.* Optical Materials Express, 2020. **10**(7): p. 1509-1521.
30. Uhlmann, D.R. and N.J. Kreidl. *Optical properties of glass*. 1991.
31. Yablon, A.D., *Optical and mechanical effects of frozen-in stresses and strains in optical fibers.* IEEE Journal of Selected Topics in Quantum Electronics, 2004. **10**(2): p. 300-311.
32. Roselló-Mechó, X., et al., *Measurement of Pockels' coefficients and demonstration of the anisotropy of the elasto-optic effect in optical fibers under axial strain.* Optics Letters, 2016. **41**(13): p. 2934-2937.
33. Ryan, C., et al., *Pockels Coefficients in Multicomponent Oxide Glasses.* International Journal of Applied Glass Science, 2015. **6**(4): p. 387-396.
34. Malitson, I.H., *Interspecimen Comparison of the Refractive Index of Fused Silica*,†.* Journal of the Optical Society of America, 1965. **55**(10): p. 1205-1209.
35. Fleming, J.W. *Material dispersion in lightguide glasses*. Electronics Letters, 1978. **14**, 326-328.
36. Leviton, D.B. and B.J. Frey. *Temperature-dependent absolute refractive index measurements of synthetic fused silica*. in *Proceedings of SPIE - The International Society for Optical Engineering*. 2006.
37. Yablon, A.D., et al., *Refractive index perturbations in optical fibers resulting from frozen-in viscoelasticity.* Applied Physics Letters, 2004. **84**(1): p. 19-21.
38. Hibino, Y., F. Hanawa, and M. Horiguchi, *Drawing-induced residual stress effects on optical characteristics in pure-silica-core single-mode fibers.* Journal of Applied Physics, 1989. **65**(1): p. 30-34.
39. Anuszkiewicz, A., et al., *Experimental analysis of axial stress distribution in nanostructured core fused silica fibers.* Optical Materials Express, 2019. **9**(11): p. 4370-4378.
40. Kawachi, M., T. Edahiro, and H. Toba *Microlens formation on VAD single-mode fibre ends*. Electronics Letters, 1982. **18**, 71-72.
41. Devyatykh, G.G., et al., *Material dispersion and Rayleigh scattering in glassy germanium dioxide, a substance with promising applications in low-loss optical fiber waveguides.* Soviet Journal of Quantum Electronics, 1980. **10**(7): p. 900.
42. Grobnic, D., et al., *Type I and II Bragg gratings made with infrared femtosecond radiation in high and low alumina content aluminosilicate optical fibers.* Optica, 2015. **2**(4): p. 313-322.
43. Cavillon, M., P.D. Dragic, and J. Ballato, *Additivity of the coefficient of thermal expansion in silicate optical fibers.* Optics Letters, 2017. **42**(18): p. 3650-3653.
44. Dragic, P.D., et al., *A unified materials approach to mitigating optical nonlinearities in optical fiber. II. A. Material additivity models and basic glass properties.* International Journal of Applied Glass Science, 2018. **9**(2): p. 278-287.
45. Dianov, E.M. and V.M. Mashinsky, *Germania-based core optical fibers.* Journal of Lightwave Technology, 2005. **23**(11): p. 3500-3508.
46. Erdogan, T., *Fiber grating spectra.* Journal of Lightwave Technology, 1997. **15**(8): p. 1277-1294.
47. Pal, S., et al., *Characteristics of potential fibre Bragg grating sensor-based devices at elevated temperatures.* Measurement Science and Technology, 2003. **14**(7): p. 1131.
48. Soares De Lima Filho, E., et al., *Fiber Bragg gratings for low-temperature measurement.* Optics Express, 2014. **22**(22): p. 27681-27694.
49. Frazão, O. and J.L. Santos, *Simultaneous measurement of strain and temperature using a Bragg grating structure written in germanosilicate fibres.* Journal of Optics A: Pure and Applied Optics, 2004. **6**(6): p. 553.
50. Durr, F., et al., *Tomographic stress profiling of arc-induced long-period fiber gratings.* Journal of Lightwave Technology, 2005. **23**(11): p. 3947-3953.
51. Rego, G., et al., *Investigation of the long-term stability of arc-induced gratings heat treated at high temperatures.* Optics Communications, 2011. **284**(1): p. 169-171.
52. Flockhart, G.M.H., et al., *Quadratic behavior of fiber Bragg grating temperature coefficients.* Applied Optics, 2004. **43**(13): p. 2744-2751.
53. Imas, J.J., et al., *Accurate compensation and prediction of the temperature cross-sensitivity of tilted FBG cladding mode resonances.* Applied Optics, 2023. **62**(16): p. E8-E15.
54. Bruckner, R., *Properties and Structures of Vitreous Silica. II.* Journal of Non-Crystalline Solids, 1971. **5**: p. 177-216.
55. Kühn, B. and R. Schadrack, *Thermal expansion of synthetic fused silica as a function of OH content and fictive temperature.* Journal of Non-Crystalline Solids, 2009. **355**(4): p. 323-326.
56. Patrick, E., *Expansivity of fused quartz glass measured within 6 x 10^-10 /K.* 2023.
57. Okaji, M., et al., *Laser interferometric dilatometer at low temperatures: application to fused silica SRM 739.* Cryogenics, 1995. **35**(12): p. 887-891.
58. Hahn, T.A. and R.K. Kirby, *Thermal Expansion of Fused Silica from 80 to 1000 K - Standard Reference Material 739.* AIP Conference Proceedings, 1972. **3**(1): p. 13-24.
59. Bennett, S.J.J.J.o.P.E.S.I., *An absolute interferometric dilatometer.* 1977. **10**: p. 525-530.
60. Birch, K.P., *An automatic absolute interferometric dilatometer.* Journal of Physics E: Scientific Instruments, 1987. **20**(11): p. 1387.

61. Berthold, J.W. and S.F. Jacobs, *Ultraprecise thermal expansion measurements of seven low expansion materials.* Applied Optics, 1976. **15**(10): p. 2344-2347.
62. Wang, H., N. Yamada, and M. Okaji, *Precise Dilatometric Measurements of Silica Glasses.* Netsu Bussei, 1999. **13**(1): p. 17-22.
63. White, T.H.K.B.a.G.K., *Heat capacity and thermal expansion at low temperatures*. International cryogenics monograph series. 1999: New York : Kluwer Academic/Plenum.
64. Gulati, S.T. and J.D. Helfinstine, *Fatigue Behavior of GeO2-SiO2 Glasses.* MRS Online Proceedings Library, 1998. **531**(1): p. 133-141.
65. Riebling, E.F., *Nonideal Mixing in Binary Ge0,-SiO, Glasses.* Journal of the American Ceramic Society, 1968. **51**(7): p. 406-407.
66. Huang, Y.Y., A. Sarkar, and P.C. Schultz, *Relationship between composition, density and refractive index for germania silica glasses.* Journal of Non-Crystalline Solids, 1978. **27**(1): p. 29-37.
67. Mackenzie, J.D., *Density and Expansivity of Vitreous Germania.* Journal of the American Ceramic Society, 1959. **42**(6): p. 310-310.
68. Napolitano, A. and P.B. Macedo, *Spectrum of Relaxation Times in GeO(2) Glass.* (0022-4332 (Print)).
69. Adamovsky, G., et al., *Peculiarities of thermo-optic coefficient under different temperature regimes in optical fibers containing fiber Bragg gratings.* Optics Communications, 2012. **285**(5): p. 766-773.
70. Sánchez, L.A., et al., *High accuracy measurement of Poisson's ratio of optical fibers and its temperature dependence using forward-stimulated Brillouin scattering.* Optics Express, 2022. **30**(1): p. 42-52.
71. Jog, E.S. and R.S. Krishnan, *Dispersion of the Photoelastic Constants of Fused Silica.* Nature, 1957. **179**(4558): p. 540-541.
72. Biegelsen, D.K. and J.C. Zesch, *Optical frequency dependence of the photoelastic coefficients of fused silica.* Journal of Applied Physics, 1976. **47**(9): p. 4024-4025.
73. Jenkins, A., et al., *Wavelength-dependent elasto-optic tensor elements from acoustic Bragg diffraction.* Journal of Non-Crystalline Solids, 2023. **620**: p. 122580.
74. Martina, D.-P., et al., *Whispering Gallery Modes for Accurate Characterization of Optical Fibers' Parameters*, in *Applications of Optical Fibers for Sensing*, C.-L. Christian, Editor. 2018, IntechOpen: Rijeka. p. Ch. 8.
75. Barlow, A. and D. Payne, *The stress-optic effect in optical fibers.* IEEE Journal of Quantum Electronics, 1983. **19**(5): p. 834-839.
76. Bertholds, A. and R. Dandliker, *Determination of the individual strain-optic coefficients in single-mode optical fibres.* Journal of Lightwave Technology, 1988. **6**(1): p. 17-20.
77. Schuh, R.E., S. Xuekang, and A.S. Siddiqui, *Polarization mode dispersion in spun fibers with different linear birefringence and spinning parameters.* Journal of Lightwave Technology, 1998. **16**(9): p. 1583-1588.
78. Sánchez, L.A., et al., *Strain and temperature measurement discrimination with forward Brillouin scattering in optical fibers.* 2022. **30 9**: p. 14384-14392.
79. Zou, W., Z. He, and K. Hotate, *Investigation of Strain- and Temperature-Dependences of Brillouin Frequency Shifts in GeO$_{2}$ -Doped Optical Fibers.* Journal of Lightwave Technology, 2008. **26**(13): p. 1854-1861.
80. Deroh, M., et al., *Large Brillouin gain in Germania-doped core optical fibers up to a 98 mol% doping level.* Optics Letters, 2018. **43**(16): p. 4005-4008.
81. Beugnot, J.-C. and V. Laude, *Electrostriction and guidance of acoustic phonons in optical fibers.* Physical Review B, 2012. **86**(22): p. 224304.
82. Lambin-Iezzi, V., et al., *Stimulated Brillouin scattering in SM ZBLAN fiber.* Journal of Non-Crystalline Solids, 2013. **359**: p. 65-68.
83. Zou, W., et al., *Dependence of Brillouin Frequency Shift in Optical Fibers on Draw-Induced Residual Elastic and Inelastic Strains.* IEEE Photonics Technology Letters, 2007. **19**(18): p. 1389-1391.
84. Le Parc, R., et al., *Influence of fictive temperature and composition of silica glass on anomalous elastic behaviour.* Journal of Physics: Condensed Matter, 2006. **18**(32): p. 7507.
85. Thomas, P.J.S., et al., *Normal acoustic modes and Brillouin scattering in single-mode optical fibers.* 1979. **19**: p. 4986-4998.
86. Zou, W., Z. He, and K. Hotate, *Two-Dimensional Finite-Element Modal Analysis of Brillouin Gain Spectra in Optical Fibers.* IEEE Photonics Technology Letters, 2006. **18**(23): p. 2487-2489.
87. Dragic, P.D., *Brillouin spectroscopy of Nd–Ge co-doped silica fibers.* Journal of Non-Crystalline Solids, 2009. **355**(7): p. 403-413.
88. Koyamada, Y., et al., *Simulating and designing Brillouin gain spectrum in single-mode fibers.* Journal of Lightwave Technology, 2004. **22**(2): p. 631-639.
89. Jen, C.-K., et al., *Acoustic Characterization of Silica Glasses.* Journal of the American Ceramic Society, 1993. **76**(3): p. 712-716.
90. Nikles, M., L. Thevenaz, and P.A. Robert, *Brillouin gain spectrum characterization in single-mode optical fibers.* Journal of Lightwave Technology, 1997. **15**(10): p. 1842-1851.
91. Lagakos, N., J.A. Bucaro, and R. Hughes, *Acoustic sensitivity predictions of single-mode optical fibers using Brillouin scattering.* Applied Optics, 1980. **19**(21): p. 3668-3670.

92. Munro, R.G. *Elastic Moduli Data for Polycrystalline Oxide Ceramics | NIST*. 2002.
93. Clowes, J.R., S. Syngellakis, and M.N. Zervas, *Pressure sensitivity of side-hole optical fiber sensors.* IEEE Photonics Technology Letters, 1998. **10**(6): p. 857-859.
94. Li, P., et al. *A Nondestructive Measurement Method of Optical Fiber Young's Modulus Based on OFDR*. Sensors, 2022. **22**, DOI: 10.3390/s22041450.
95. Antunes, P., et al., *Elastic constant measurement for standard and photosensitive single mode optical fibres.* Microwave and Optical Technology Letters, 2008. **50**(9): p. 2467-2469.
96. Suito, K., et al., *Elastic Properties of Obsidian, Vitreous SiO2, and Vitreous GeO2 under High Pressure up to 6 GPa*, in *High-Pressure Research: Application to Earth and Planetary Sciences*. 1992. p. 219-225.
97. Makishima, A. and J.D. Mackenzie, *Calculation of bulk modulus, shear modulus and Poisson's ratio of glass.* Journal of Non-Crystalline Solids, 1975. **17**(2): p. 147-157.
98. Rocherulle, J., et al., *Elastic moduli of oxynitride glasses: Extension of Makishima and Mackenzie's theory.* Journal of Non-Crystalline Solids, 1989. **108**(2): p. 187-193.
99. Dragic, P.D., *The Acoustic Velocity of Ge-Doped Silica Fibers: A Comparison of Two Models.* International Journal of Applied Glass Science, 2010. **1**(3): p. 330-337.
100. Urbanczyk, W., T. Martynkien, and W.J. Bock, *Dispersion effects in elliptical-core highly birefringent fibers.* Applied Optics, 2001. **40**(12): p. 1911-1920.
101. Galtarossa, A., D. Grosso, and L. Palmieri, *Accurate Characterization of Twist-Induced Optical Activity in Single-Mode Fibers by Means of Polarization-Sensitive Reflectometry.* IEEE Photonics Technology Letters, 2009. **21**(22): p. 1713-1715.
102. Galtarossa, A. and L. Palmieri, *Measure of twist-induced circular birefringence in long single-mode fibers: theory and experiments.* Journal of Lightwave Technology, 2002. **20**(7): p. 1149-1159.
103. Ivanov, O.V. *Experimental Investigation of Rotation of Polarization in Strongly Twisted Optical Fibers of Various Types*. in *2018 International Conference Laser Optics (ICLO)*. 2018.
104. El-Khozondar, H.J., et al. *Experimental investigation of polarization rotation in twisted optical fibers*. in *2009 International Symposium on Optomechatronic Technologies*. 2009.
105. Roths, J. and F. Jülich. *Determination of strain sensitivity of free fiber Bragg gratings*. in *Photonics Europe*. 2008.
106. Jülich, F., et al., *Gauge factors of fibre Bragg grating strain sensors in different types of optical fibres.* Measurement Science and Technology, 2013. **24**(9): p. 094007.
107. Acheroy, S., et al., *Algorithms for determining the radial profile of the photoelastic coefficient in glass and polymer optical fibers.* Optics Express, 2015. **23**(15): p. 18943-18954.
108. Namihira, Y., *Opto-elastic constant in single mode optical fibers.* Journal of Lightwave Technology, 1985. **3**(5): p. 1078-1083.
109. Sinha, N.K., *Normalised dispersion of birefringence of quartz and stress optical coefficient of fused silica and plate glass.* Physics and Chemistry of Glasses, 1978. **19**(4): p. 69-77.
110. Primak, W. and D. Post, *Photoelastic Constants of Vitreous Silica and Its Elastic Coefficient of Refractive Index.* Journal of Applied Physics, 1959. **30**(5): p. 779-788.
111. RIEBLING, E.F., *Nonideal Mixing in Binary Ge0,-SiO, Glasses.* 1968. **51**(7): p. 406-407.
112. Huang, Y., A. Sarkar, and P.J.J.o.N.-C.S. Schultz, *Relationship between composition, density and refractive index for germania silica glasses.* 1978. **27**(1): p. 29-37.
113. MACKENZIE, J.D., *Density and Expansivity of Vitreous Germania.* 1959. **42**(6): p. 310-310.
114. Doweidar, H., *Considerations on the structure and physical properties of B2O3–SiO2 and GeO2–SiO2 glasses.* Journal of Non-Crystalline Solids, 2011. **357**(7): p. 1665-1670.
115. Napolitano A, M.P., *Spectrum of Relaxation Times in GeO2 Glass.* J Res Natl Bur Stand A Phys Chem. , 1968. **72**(4): p. 425-433.
116. Spinner, S. and G.W. Cleek, *Temperature Dependence of Young's Modulus of Vitreous Germania and Silica.* Journal of Applied Physics, 1960. **31**(8): p. 1407-1410.
117. KRAUSE, J.T. and C.R. KURKJIAN, *Vibrational Anomalies in Inorganic Glass Formers.* 1968. **51**(4): p. 226-227.
118. Shelby, J.E., *Properties and structure of B2O3–GeO2 glasses.* Journal of Applied Physics, 1974. **45**(12): p. 5272-5277.
119. Filho, E.S.d.L., et al., *Fiber Bragg gratings for low-temperature measurement.* Optics Express, 2014. **22**(22): p. 27681-27694.
120. Wenyuan, W., et al. *Measurements of thermo-optic coefficient of standard single mode fiber in large temperature range*. in *Proc.SPIE*. 2015.
121. Wang, W., et al. *Fiber-Optic Intrinsic Fabry-Perot Temperature Sensor Fabricated by Femtosecond Lasers*. in *Optical Sensors and Biophotonics II*. 2010. Shanghai: Optica Publishing Group.
122. Chang, S., et al., *Heterodyne interferometric measurement of the thermo-optic coefficient of single mode fiber.* 2000. **38**(3): p. 437-442.
123. Li, L., et al., *FFPI-FBG hybrid sensor to measure the thermal expansion and thermo-optical coefficient of a silica-based fiber at cryogenic temperatures.* Chinese Optics Letters, 2015. **13**(10): p. 100601.

 doi:10.20944/preprints202407.0272.v1

124. Gao, H., et al., *Investigation on the Thermo-Optic Coefficient of Silica Fiber Within a Wide Temperature Range.* Journal of Lightwave Technology, 2018. **36**(24): p. 5881-5886.
125. Du, Y., et al., *Cryogenic Temperature Measurement Using Rayleigh Backscattering Spectra Shift by OFDR.* IEEE Photonics Technology Letters, 2014. **26**(11): p. 1150-1153.
126. Kreger, S.T., et al. *High Resolution Distributed Strain or Temperature Measurements in Single-and Multi-mode Fiber Using Swept-Wavelength Interferometry*. in *Optical Fiber Sensors*. 2006. Cancun: Optica Publishing Group.
127. Chaccour, L., *Rayleigh Backscattered Signal Enhancement in Highly GeO_2-Doped-Core Silica Fibers.* IEEE Photonics Technology Letters, 2022. **34**(6): p. 345-348.
128. Terra, O., *Optoelectronic oscillations for thermo-optic coefficient measurement of optical fibers.* Measurement Science and Technology, 2019. **30**(3): p. 035205.
129. Zou, X., et al., *Optoelectronic Oscillators (OEOs) to Sensing, Measurement, and Detection.* IEEE Journal of Quantum Electronics, 2016. **52**(1): p. 1-16.